AJNR

This information is current as of August 1, 2025.

Quantitative Blood Flow Measurements in Gliomas Using Arterial Spin-Labeling at 3T: Intermodality Agreement and Inter- and Intraobserver Reproducibility Study

T. Hirai, M. Kitajima, H. Nakamura, T. Okuda, A. Sasao, Y. Shigematsu, D. Utsunomiya, S. Oda, H. Uetani, M. Morioka and Y. Yamashita

T. Hirai
M. Kitajima
H. Nakamura
T. Okuda
A. Sasao
Y. Shigematsu
D. Utsunomiya
S. Oda
H. Uetani
M. Morioka
Y. Yamashita

Quantitative Blood Flow Measurements in Gliomas Using Arterial Spin-Labeling at 3T: Intermodality Agreement and Inter- and Intraobserver Reproducibility Study

BACKGROUND AND PURPOSE: QUASAR is a particular application of the ASL method and facilitates the user-independent quantification of brain perfusion. The purpose of this study was to assess the intermodality agreement of TBF measurements obtained with ASL and DSC MR imaging and the inter- and intraobserver reproducibility of glioma TBF measurements acquired by ASL at 3T.

MATERIALS AND METHODS: Two observers independently measured TBF in 24 patients with histologically proved glioma. ASL MR imaging with QUASAR and DSC MR imaging were performed on 3T scanners. The observers placed 5 regions of interest in the solid tumor on rCBF maps derived from ASL and DSC MR images and 1 region of interest in the contralateral brain and recorded the measured values. Maximum and average sTBF values were calculated. Intermodality and intra- and interobsever agreement were determined by using 95% Bland-Altman limits of agreement and ICCs.

RESULTS: The intermodality agreement for maximum sTBF was good to excellent on DSC and ASL images; ICCs ranged from 0.718 to 0.884. The 95% limits of agreement ranged from 59.2% to 65.4% of the mean. ICCs for intra- and interobserver agreement for maximum sTBF ranged from 0.843 to 0.850 and from 0.626 to 0.665, respectively. The reproducibility of maximum sTBF measurements obtained by methods was similar.

CONCLUSIONS: In the evaluation of sTBF in gliomas, ASL with QUASAR at 3T yielded measurements and reproducibility similar to those of DSC perfusion MR imaging.

ABBREVIATIONS: AIF = arterial input function; ASL = arterial spin-labeling; DSC = dynamic susceptibility contrast-enhanced; ICC = intraclass correlation coefficient; QUASAR = quantitative STAR labeling of arterial regions; QUIPPS = quantitative imaging of perfusion using a single subtraction; rCBF = relative cerebral blood flow; rCBV = relative cerebral blood volume; sTBF = standardized TBF; TBF = tumor blood flow

Perfusion MR imaging with the DSC method is widely used to assess the perfusion of gliomas and the degree of tumor angiogenesis, an important marker for tumor grading, therapeutic response, and prognosis of patients with these tumors.[1-7]

Perfusion MR imaging with ASL is another method to measure perfusion; magnetically labeled blood water is the endogenous tracer.[8,9] This technique has been used to evaluate perfusion in pathologic conditions.[10,11] The usefulness of perfusion MR imaging with ASL for the assessment of brain tumor angiogenesis and glioma grading[12-15] has been evaluated. The application of ASL has been restricted to specialty centers due to its low signal intensity–to-noise ratio and potential issues involving user-dependent analyses in the acquisition of quantitative rCBF measurements.[16,17]

QUASAR is a particular application of the ASL method; it facilitates the user-independent quantification of rCBF and yielded good reproducibility in healthy volunteers.[16,17] To our knowledge, the reliability and reproducibility of glioma perfusion values obtained by ASL with QUASAR have not been reported. We evaluated the intermodality agreement of TBF measurements obtained with QUASAR and DSC MR imaging and the inter- and intraobserver reproducibility of glioma TBF measurements acquired by QUASAR at 3T.

Materials and Methods

Patients

The institutional review board of Kumamoto University Hospital approved this retrospective study and waived patient informed consent for the use of their MR images. This study included 24 consecutive patients with histologically proved supratentorial gliomas; their initial preoperative MR images were used. Tissues for histologic analysis were obtained at stereotactic biopsy or tumor resection. All gliomas were classified according to the 2007 World Health Organization brain tumor classification.[18] Histopathologically, 18 tumors were glioblastomas, 2 each were anaplastic oligodendrogliomas and oligoastrocytomas, and 1 each was an anaplastic astrocytoma and a diffuse astrocytoma. The patients were 14 men and 10 women; their mean age was 58.4 years ± 16.6 (range, 31–81 years).

MR Imaging Protocol

Conventional MR Imaging and DSC Perfusion MR Imaging. All DSC perfusion MR imaging studies were performed on a 3T MR imaging system (Magnetom Trio, A Tim; Siemens, Erlangen, Germany) by using a 12-channel head coil. Before DSC perfusion MR imaging, conventional transverse T1-weighted (TR/TE, 600/8.5 ms), T2-weighted (TR/TE, 3600/96 ms; echo-train length, 7), and fluid-attenuated inversion recovery (TR/TE, 10 000/120 ms; TI, 2800 ms) sequences were performed at a section thickness of 5 mm.

A preloading dose of gadopentate dimeglumine (Magnevist, 0.06 mmol/kg of body weight; Bayer-Schering, Berlin, Germany) was injected before DSC scan acquisition to correct for T1-weighted leakage effects that might result in TBF underestimation.[19] DSC perfusion MR imaging was performed during the injection of a bolus of gadopentate dimeglumine (Magnevist, 0.07 mmol/kg body weight) at a rate of 3 mL/s through a 20-ga intravenous catheter; this was immediately followed by a bolus injection of saline (3 mL/s, total 20 mL). DSC perfusion MR imaging scans were acquired with a single-shot gradient-echo echo-planar imaging sequence (TR/TE, 1400/32 ms; flip angle, 60°; FOV, 23 cm; matrix, 128 × 128; section thickness/gap, 5/1 mm; in-plane resolution, 1.8 × 1.8 mm; acquisition time, 1 minute 17 seconds). A total of 50 dynamic series of 19 sections to cover the entire brain were obtained. Subsequently, transverse T1-weighted (TR/TE, 600/8.5 ms) and magnetization-prepared rapid acquisition of gradient echo (TR/TE, 1900/4.7 ms; TI, 900 seconds) sequences were performed. To analyze TBF from DSC perfusion MR imaging data, we used commercially available built-in software (Siemens). For DSC perfusion MR imaging, AIFs were manually defined by 1 radiologist and 1 technologist and by selecting 10–16 pixels containing the M1 or M2 segment of the middle cerebral artery in the Sylvian fissure. Each pixel was confirmed to contain the middle cerebral artery by its anatomic location and by a susceptibility time curve exhibiting a steeper slope and greater amplitude than in the adjacent brain parenchyma.

ASL Perfusion MR Imaging. ASL perfusion MR imaging studies were performed 1–7 days later (mean, 3 days). All ASL perfusion MR imaging studies were on a 3T MR imaging unit (Achieva 3T; Philips Healthcare, Best, the Netherlands) by using an 8-channel head-array receiving coil for sensitivity encoding parallel imaging. ASL was with the application of QUASAR, a multisection multiple-time-points−capable ASL sequence based on pulsed ASL principles.[16] Details on the sequence and the calculation of the perfusion parameters have been described elsewhere.[16] Both labeling and control experiments were preceded by a saturation pulse; QUIPSS II-type bolus saturation was applied during Look-Locker sampling.[20,21] In addition, both crushed and noncrushed control-label pairs were acquired in an interleaved manner on a voxel-by-voxel basis for AIF.[16]

On the basis of conventional MR imaging results, we selected 7 transverse sections through the tumor for our ASL studies. The imaging parameters for the ASL sequence with QUASAR were the following: TR/TE, 3000/24 ms; flip angle, 30°; sensitivity encoding factor, 2.5; FOV, 23 × 23 cm; matrix, 64 × 64; in-plane resolution, 3.59 × 3.59 mm; and section thickness/gap, 6/2 mm. The first labeling delay time (TI_1) of the multiple-time-points ASL sequence was 40 ms; 7 different phase data were acquired at 7 different labeling delay time points every 250 ms ($\Delta TI = 250$ ms). A total of 49 images, labeled subtracted from nonlabeled images, were obtained. The labeling slab thickness was 150 mm; it was positioned at the level of the upper cervical region. The total acquisition time was 5 minutes 52 seconds.

The ASL imaging data were transferred to an off-line workstation (Precision 530; Dell, Round Rock, Texas); Philips Research Imaging Development Environment software (Philips Healthcare) was used for constructing rCBF maps.

Image Evaluation

Two board-certified radiologists (T.O. and M.K. with 21 and 18 years of experience in neuroradiologic MR imaging, respectively) independently evaluated the conventional MR imaging, DSC, and ASL perfusion MR imaging data on a PACS workstation; they were blinded to the clinical and histopathologic results. Each observer participated in 3 review sessions held at 4-week intervals. In the first session, conventional MR imaging and DSC rCBF maps were evaluated with built-in software on the PACS workstation. In the second and third sessions, conventional MR images and ASL rCBF maps were assessed on the same PACS workstation, and ASL rCBF maps were analyzed with ImageJ software (National Institutes of Health, Bethesda, Maryland). The software allowed the enlargement of regions of special interest in any given spatial orientation. To minimize confounding factors in the TBF analysis, the region-of-interest size in the lesion and contralateral normal brain was kept constant (radius = 1 pixel of the ASL image, 3.6 mm) on both ASL and DSC images.

Each observer placed 5 regions of interest within solid tumor components where it was thought that high rCBF values would be found; they also placed 1 region of interest in the contralateral reference brain on ASL and DSC rCBF maps (Fig 1). The rCBF values in all regions of interest were recorded. To place the region of interest correctly in the solid portion of the tumor while avoiding volume-averaging with normal vessels that influence rCBF values, the observers carefully inspected conventional MR images. The maximum sTBF value was calculated as the highest rCBF in the solid tumor divided by the rCBF in the contralateral reference brain. Average sTBF values were calculated as the mean of 5 rCBFs in the solid tumor divided by the rCBF in the contralateral reference brain.

Statistical Analysis

The difference in maximum and average sTBF values on DSC and ASL images was evaluated with the paired t test. To assess the presence of any systematic bias in the sTBF measurements on repeated ASL scans, we compared sTBF values on the first and second ASL scans, by using the paired t test.

For each DSC imaging pair, interobserver agreement was assessed with the ICC.[22,23] To determine the intermodality agreement of sTBF measurements, we averaged the observers' measurements of maximum and average sTBF values on DSC images and used these as representative DSC imaging data. For each ASL imaging pair, intra- and interobserver agreement was assessed with the ICC, in which ICC < 0.40 = poor, 0.40−0.59 = fair, 0.60−0.74 = good, and ICC > 0.74 = excellent.[22] The intermodality agreement of sTBF measurements was evaluated with the ICC; the difference in ICCs was compared by using the Z-test.[24,25]

To estimate the magnitude of changes in the sTBF value that can be detected confidently in a single individual, the 95% limits of agreement between the sTBF value measured on the first and second ASL image sets were obtained by using the Bland-Altman method[26]; the results were expressed as a percentage of mean sTBF values. For the DSC image sets, we also obtained the 95% limits of agreement in the sTBF values recorded by the 2 readers by using the Bland-Altman method.

Statistical analyses were with commercial software (Statistical Package for the Social Sciences, Version 18, SPSS, Chicago, Illinois;
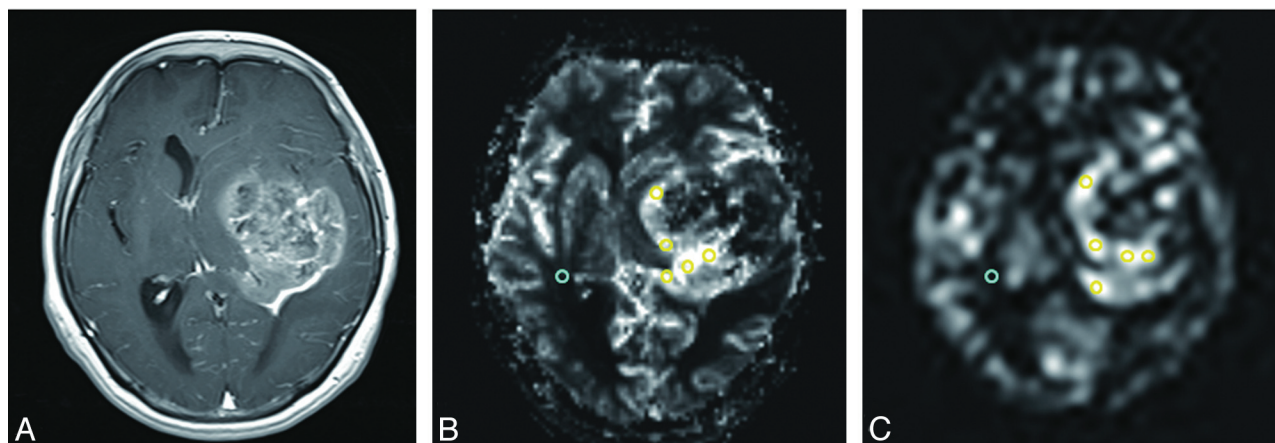
Fig 1. MR images of a 58-year-old woman with glioblastoma. *A,* Axial contrast-enhanced T1-weighted image shows a heterogeneous ring-enhanced lesion in the left basal ganglia. rCBF maps derived from DSC (*B*) and ASL images (*C*). The MR imaging data indicate a hyperperfused lesion. Two observers placed 5 regions of interest (yellow circle) within solid tumor components and 1 region of interest (blue circle) in the contralateral brain on each rCBF map.

Table 1: sTBF measurements of 24 gliomas for 2 observers

	Observer 1	Observer 2
DSC		
Maximum	4.129 ± 2.839	3.897 ± 1.943
Average	3.872 ± 2.727	3.240 ± 1.814
ASL		
Maximum		
First	3.840 ± 2.335	3.599 ± 1.572
Second	3.712 ± 2.068	3.461 ± 1.549
Average		
First	3.101 ± 1.828	2.805 ± 1.270[a]
Second	3.095 ± 1.855	2.717 ± 1.301[a]

[a] $P < .05$ compared with mean-maximum or average sTBF, in which 2 observers' measurements on DSC images were averaged by using a paired *t* test.

MedCalc for Windows, MedCalc Software, Mariakerke, Belgium). A *P* value < .05 was considered to indicate significant differences.

Results

Twenty-four target lesions in 24 patients (1 lesion per patient) were evaluated. The mean diameter of the lesions was 47.4 ± 15.1 mm (range, 20.1–86.3 mm); 20 lesions (83.3%) were contrast-enhanced.

The sTBF values of the 24 gliomas are summarized in Table 1. On DSC images, there was no significant difference in the mean-maximum and average sTBF values recorded by the 2 observers. The ICC with a 95% confidence interval for interobserver agreement on DSC imaging sets was good; it was 0.728 with 0.3706–0.8822 for maximum sTBF and 0.711 with 0.3329–0.8752 for average sTBF values. The 95% limits of agreement in maximum and average sTBF values between the

2 observers were 81.5% and 82.9% of the mean sTBF values, respectively. The means of the maximum and average sTBF values, averaging the observers' measurements on DSC images, were 4.042 ± 2.154 and 3.568 ± 2.031, respectively.

Although the mean-maximum sTBF measured by the 2 observers was slightly higher for DSC than ASL images, the differences were not statistically significant (Table 1). On the other hand, the measured mean average sTBF for observer 2 was significantly higher for DSC than for ASL images (first set, $P = .009$; second set, $P = .004$). On the first and second ASL imaging set, there was no significant difference in the mean-maximum and average sTBF recorded by the 2 observers.

The intermodality agreement for maximum and average sTBF measurements on DSC and ASL images was good to excellent; the ICC ranged from 0.718 to 0.884 and from 0.698 to 0.798, respectively (Table 2). There was no significant difference in the ICC between DSC and ASL images for either observer. The 95% limits of agreement between sTBF measured on DSC and ASL images ranged from 59.2% to 65.4% of the mean sTBF for maximum sTBF and from 60.1% to 75.2% of the mean sTBF for average sTBF values (Table 2 and Fig 2).

The intraobserver reproducibility of the maximum and average sTBF measurements on ASL images was excellent; the ICC ranged from 0.843 to 0.850 and from 0.872 to 0.927, respectively (Table 3). There was no significant difference in the ICC between the first and second set. The 95% limits of agreement between sTBF measured on repeated ASL images ranged from 39.7% to 58.8% of the mean sTBF for maximum and from 38.0% to 46.0% of the mean sTBF for average sTBF (Fig 3).

Table 2: Intermodality agreement of sTBF measurements

	Observer 1		Observer 2	
	Maximum TBF	Average TBF	Maximum TBF	Average TBF
ICC[a]				
First	0.884 (0.751–0.948)	0.798 (0.588–0.908)	0.749 (0.503–0.883)	0.698 (0.417–0.857)
Second	0.798 (0.588–0.907)	0.745 (0.495–0.881)	0.718 (0.443–0.865)	0.714 (0.443–0.865)
95% limits of agreement[b]				
First	64.7	75.2	59.2	67.8
Second	65.4	71.1	61.2	60.1

[a] Data in parentheses are 95% confidence intervals.
[b] Expressed as a percentage of the mean.
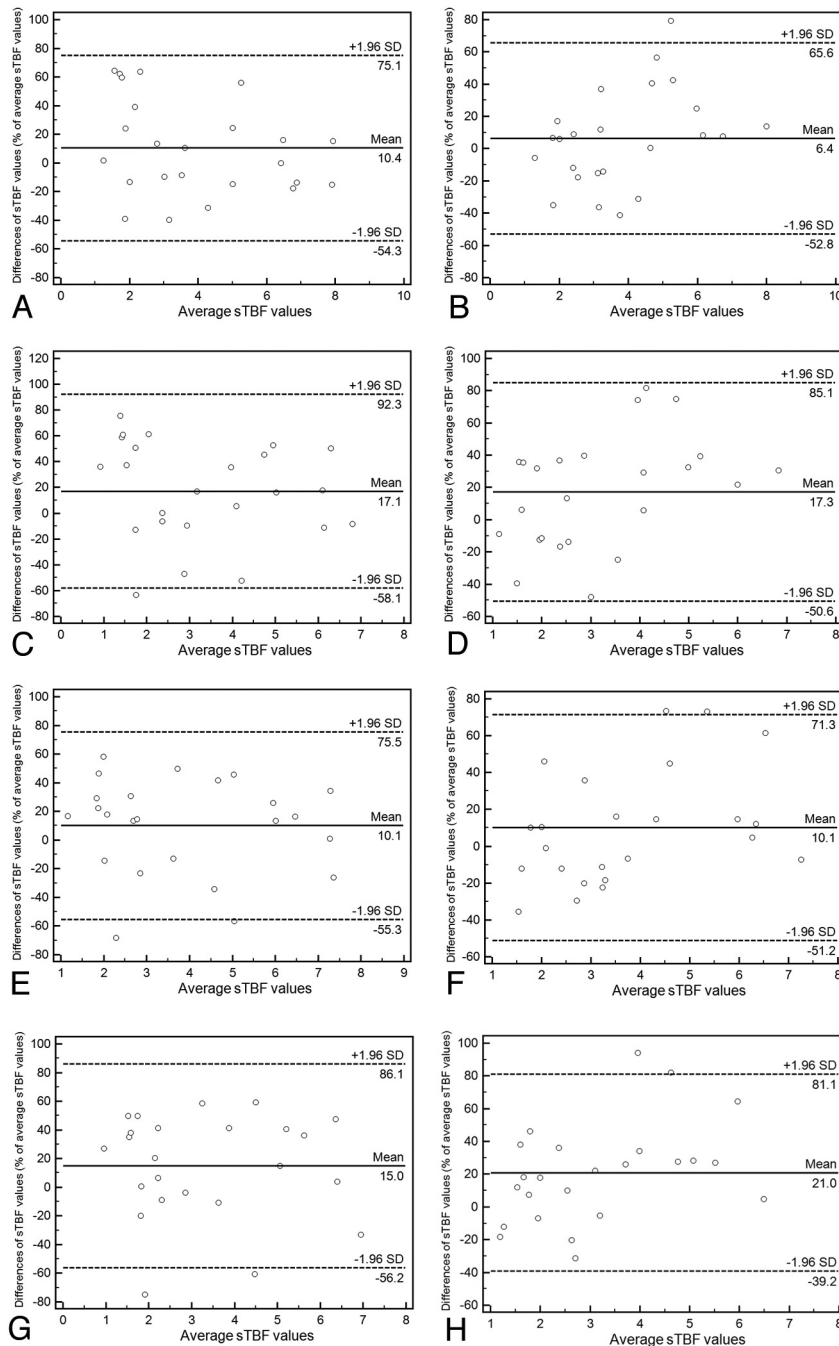
Fig 2. Bland-Altman plots showing intermodality variability of sTBF measurements for observers 1 (*A, C, E,* and *G*) and 2 (*B, D, F,* and *H*) with maximum (*A, B, E,* and *F*) and average methods (*C, D, G,* and *H*) at the first (*A, B, C,* and *D*) and second (*E, F, G,* and *H*) reading. The x-axes show the mean values of sTBF measured on DSC and ASL images. The y-axes show the difference between sTBF values for each set as a percentage of their mean. *A,* Intermodality variability for observer 1, first reading, and maximum sTBF measurements. *B,* Intermodality variability for observer 2, first reading, and maximum sTBF measurements. *C,* Intermodality variability for observer 1, first reading, and average sTBF measurements. *D,* Intermodality variability for observer 2, first reading, and average sTBF measurements. *E,* Intermodality variability for observer 1, second reading, and maximum sTBF measurements. *F,* Intermodality variability for observer 2, second reading, and maximum sTBF measurements. *G,* Intermodality variability for observer 1, second reading, and average sTBF measurements. *H,* Intermodality variability for observer 2, second reading, and average sTBF measurements. Solid lines indicate mean absolute differences (ie, bias); dashed lines, 95% limits of agreement.

The interobserver agreement for maximum and average sTBF measurements on ASL images was good for maximum and average sTBF; the ICC ranged from 0.626 to 0.665 and from 0.622 to 0.643, respectively (Table 4). There were no significant differences in the ICC between the 2 observers. The 95% limits of agreement between the sTBFs measured by the 2 observers ranged from 78.7% to 87.0% of the mean sTBF for maximum and from 78.5% to 88.9% of the mean sTBF for average sTBF values (Fig 4).

Discussion

ASL is a promising tool for assessing tumor angiogenesis and for glioma grading.[12-15] However, for ASL to be practical in determining changes in tumor rCBF values, the reproducibility of rCBF measurements must be ascertained. We found that the maximum sTBF values measured with ASL by using QUASAR agreed well with the values obtained by DSC perfusion MR imaging; the difference in sTBF values acquired by the 2 methods was within a similar range. Thus, ASL by using

Table 3: Intraobserver reproducibility of sTBF measurements

	Observer 1		Observer 2	
	Maximum TBF	Average TBF	Maximum TBF	Average TBF
ICC[a]	0.843 (0.672–0.929)	0.927 (0.839–0.968)	0.850 (0.684–0.932)	0.872 (0.727–0.943)
95% limits of agreement[b]	58.8	46.0	39.7	38.0

[a] Data in parentheses are 95% confidence intervals.
[b] Expressed as a percentage of the mean.

QUASAR may represent a reliable technique for evaluating brain tumor perfusion and an alternative to the DSC method in the quantitative evaluation of glioma perfusion. We attribute the good intermodality agreement to the high quality of data obtained with the QUASAR technique.

An earlier study that used 1.5T pulsed ASL performed at a single TI point also showed a high correlation for sTBF measurements on ASL and DSC perfusion maps.[12] However, pulsed ASL with a single TI point may lead to serious errors in the estimation of perfusion due to its sensitivity to the transit time.[16] To render ASL less transit-time sensitive, bolus saturation sequences such as QUIPSS II[20] were developed. The principle of these techniques is to saturate the part of the label that remains within the labeling slab at a time delay that is short enough for the trailing edge of the fastest blood to remain within the inversion slab. However, if the transit-time distribution is wide (as in patients with atherosclerosis), these methods would not work. This problem can be solved by acquiring images at multiple TIs.

The bolus saturation techniques and the acquisition of images at multiple time points as used in the QUASAR sequence render ASL less sensitive to the transit time. In addition, the QUASAR sequence can quantify rCBF user-independently because AIF is calculated automatically voxel-by-voxel based on

crushed and noncrushed control-label pairs.[16] The high signal intensity–to-noise ratios on 3T may have also affected our results.

Our data suggest that the 95% limit of agreement in sTBF measurements is slightly greater for interobserver than intraobserver assessments. Despite our attempts for consistent region-of-interest placement, a change in sTBF measurements between 2 observers, amounting to less than approximately 89% of the mean sTBF (ie, 95% limit of agreement), was within the limit of error on ASL images. The change in sTBF between 2 observers on DSC images was also approximately 83% of the mean sTBF values. Wetzel et al,[27] who reported that the limit of error in sTBF on DSC images was relatively high, attributed the relatively large differences between observers in part to noise in both the lesions and the reference regions of interest. Thus, the error limit in our study may also be due to the effect of noise on the measurements.

For both observers, the mean-maximum and average sTBF values were higher on DSC than on ASL images. In 1 observer, there was a significant difference in average sTBF measurements on DSC and ASL images. While we cannot readily explain this, the difference in sTBF measurements between the 2 modalities may be attributable to differences in the characteristics of perfusion MR imaging. Because we used the gradient
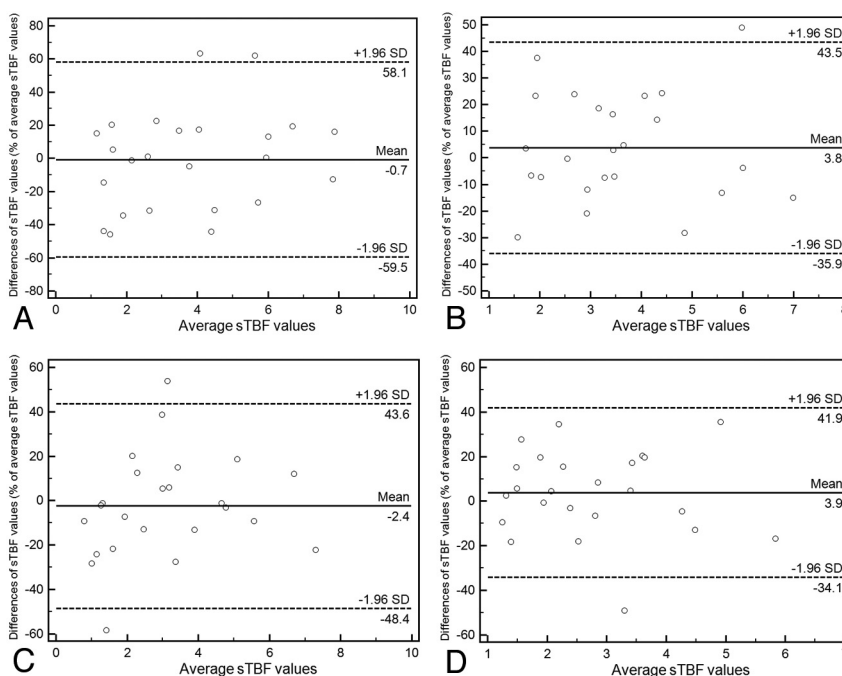
Fig 3. Bland-Altman plots showing intraobserver variability of sTBF measurements for observers 1 (*A* and *C*) and 2 (*B* and *D*) with maximum (*A* and *B*) and average methods (*C* and *D*). The x-axes show the mean values of sTBF measured on repeated ASL images; the y-axes show the difference between sTBF values for each set as a percentage of their mean. *A*, Intraobserver variability for observer 1 and maximum sTBF measurements. *B*, Intraobserver variability for observer 2 and maximum sTBF measurements. C. Intraobserver variability for observer 1 and average sTBF measurements. *D*, Intraobserver variability for observer 2 and average sTBF measurements. Solid lines indicate mean absolute differences (ie, bias); dashed lines, 95% limits of agreement.

Table 4: Interobserver agreement for sTBF measurements

	Maximum TBF		Average TBF	
	1st Reading	2nd Reading	1st Reading	2nd Reading
ICC[a]	0.665 (0.364–0.840)	0.643 (0.332–0.828)	0.626 (0.306–0.819)	0.622 (0.300–0.817)
95% limits of agreement[b]	78.7	87.0	88.9	78.5

[a] Data in parentheses are 95% confidence intervals.
[b] Expressed as a percentage of the mean.

echo−type echo-planar imaging sequence in our DSC study, large arteries would not have been suppressed.[28] On the other hand, on ASL images, large arteries were suppressed by the crusher gradients.[16] Although the observers carefully placed the region of interest inside the solid portion of the tumor while avoiding volume averaging with normal vessels, the signal intensity from large arteries could have affected the results obtained with DSC images.

Although a constant region-of-interest size was used in this study, differences in the section thickness may have affected our results. The section thickness was 6 mm for ASL and 5 mm for DSC images. The partial volume effect of normal brain tissue can be expected to exert a greater effect on ASL images, resulting in a lower signal intensity than on DSC images. Because this effect may be exacerbated with the average sTBF method, for the evaluation of sTBF in gliomas on ASL images, the maximum sTBF method may be more suitable than the average sTBF method.

Although the rCBV is usually used for evaluating the perfusion of gliomas, we used rCBF values. DSC perfusion MR imaging can provide both rCBF and rCBV of the brain. In contrast to DSC perfusion MR imaging, ASL methods measure CBF only.[29] Although attempts have been made to determine CBV with ASL techniques in animal models, they cannot

yet be applied in clinical practice.[30,31] Because earlier reports by using DSC perfusion MR imaging showed a strong correlation between the rCBV and rCBF ratios in high- and low-grade gliomas,[32,33] we used rCBF ratios to compare tumor perfusion obtained by DSC and ASL methods. On the basis of our finding that ASL at 3T yielded measurements similar to those of DSC perfusion MR imaging, we suggest that measuring rCBF ratios with ASL at 3T is useful for evaluating the perfusion of gliomas.

ASL is thought to be capable of measuring absolute CBF values. The absolute CBF values obtained with ASL may allow the comparison of different patients and of values obtained during the course of treatment in individual patients. To our knowledge, no systematic investigations by using the absolute CBF values obtained with ASL in patients with glioma have been reported. On the other hand, because there are several reports that used standardized CBF values with ASL,[12,14] we used standardized values in our study.

ASL has the advantage of being noninvasive; because it also does not require the administration of an extrinsic tracer, there is no contrast medium to affect the physical, chemical, or physiologic properties of the blood. Therefore, ASL may be especially useful in patients with glioma with renal dysfunction because they may be at risk for contrast-related nephro-
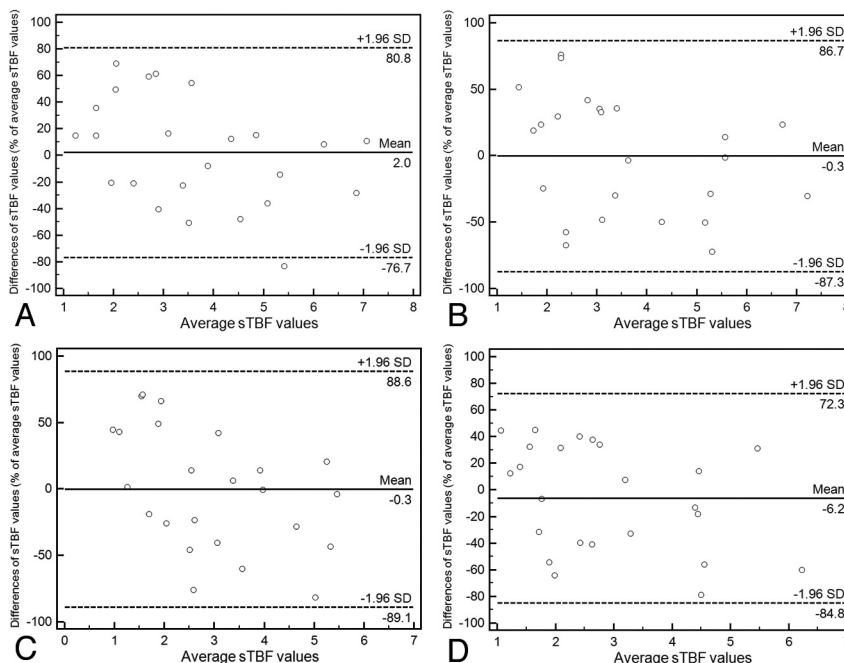
Fig 4. Bland-Altman plots showing interobserver variability of sTBF measurements for the first (*A* and *C*) and second reading (*B* and *D*) with maximum (*A* and *B*) and average methods (*C* and *D*). The x-axes show the mean sTBF values recorded by the 2 observers; the y-axes show the difference between the observers' sTBF values as a percentage of their mean. *A*, Interobserver variability for observer 1 and maximum sTBF measurements. *B*, Interobserver variability for observer 2 and maximum sTBF measurements. *C*, Interobserver variability for observer 1 and average sTBF measurements. *D*, Interobserver variability for observer 2 and average sTBF measurements. Solid lines indicate mean absolute differences (ie, bias); dashed lines, 95% limits of agreement.

genic systemic fibrosis[34] and in children in whom the rapid bolus injection of contrast materials into the vein may be difficult.

There are some limitations to this study. First, leakage of gadolinium, which occurs in most high-grade gliomas, may underestimate the rCBF at DSC perfusion MR imaging.[19] Therefore, we used the preload-correction approach, and we posit that the effect of contrast leakage on our DSC perfusion MR imaging was small. Second, CBF quantification on DSC perfusion MR imaging scans depends on the selection of the proper AIF. Although 1 experienced neuroradiologist and 1 technologist carefully selected the AIF manually, its selection on DSC images may have affected the TBF measurements. Third, we cannot rule out bias in the selection of our patients. Although our study population comprised 24 consecutive patients with histologically proved supratentorial gliomas, only 1 patient had a low-grade glioma and 4 lesions were not contrast-enhanced. Consequently, patient selection might have affected our results. Fourth, our study population was relatively small. Nevertheless, because our results were promising, further clinical studies with a larger number of patients with glioma would clarify the value of this technique in a clinical setting.

In conclusion, for the quantitative evaluation of blood flow in gliomas, ASL by using QUASAR at 3T yielded measurements and reproducibility similar to those in DSC perfusion MR imaging. Although the reproducibility of sTBF measurements by maximum and average methods was similar, the measurement method applied may affect the sTBF values of gliomas on ASL images.

References

1. Sugahara T, Korogi Y, Kochi M, et al. **Correlation of MR imaging-determined cerebral blood volume maps with histologic and angiographic determination of vascularity of gliomas.** *AJR Am J Roentgenol* 1998;171:1479–86
2. Knopp EA, Cha S, Johnson G, et al. **Glial neoplasms: dynamic contrast-enhanced T2*-weighted MR imaging.** *Radiology* 1999;211:791–98
3. Lev MH, Ozsunar Y, Henson JW, et al. **Glial tumor grading and outcome prediction using dynamic spin-echo MR susceptibility mapping compared with conventional contrast-enhanced MR: confounding effect of elevated rCBV of oligodendrogliomas.** *AJNR Am J Neuroradiol* 2004;25:214–21
4. Law M, Yang S, Babb JS, et al. **Comparison of cerebral blood volume and vascular permeability from dynamic susceptibility contrast-enhanced perfusion MR imaging with glioma grade.** *AJNR Am J Neuroradiol* 2004;25:746–55
5. Law M, Oh S, Babb JS, et al. **Low-grade gliomas: dynamic susceptibility-weighted contrast-enhanced perfusion MR imaging—prediction of patient clinical response.** *Radiology* 2006;238:658–67
6. Hirai T, Murakami R, Nakamura H, et al. **Prognostic value of perfusion MR imaging of high-grade astrocytomas: long-term follow-up study.** *AJNR Am J Neuroradiol* 2008;29:1505–10
7. Bisdas S, Kirkpatrick M, Giglio P, et al. **Cerebral blood volume measurements by perfusion-weighted MR imaging in gliomas: ready for prime time in predicting short-term outcome and recurrent disease?** *AJNR Am J Neuroradiol* 2009;30:681–88
8. Petersen ET, Zimine I, Ho YC, et al. **Non-invasive measurement of perfusion: A critical review of arterial spin labelling techniques.** *Br J Radiol* 2006;79:688–701
9. Deibler AR, Pollock JM, Kraft RA, et al. **Arterial spin-labeling in routine clin-**
10. Deibler AR, Pollock JM, Kraft RA, et al. **Arterial spin-labeling in routine clinical practice. Part 2. Hypoperfusion patterns.** *AJNR Am J Neuroradiol* 2008;29:1235–41
11. Deibler AR, Pollock JM, Kraft RA, et al. **Arterial spin-labeling in routine clinical practice. Part 3. Hyperperfusion patterns.** *AJNR Am J Neuroradiol* 2008;29:1428–35
12. Warmuth C, Gunther M, Zimmer C. **Quantification of blood flow in brain tumors: comparison of arterial spin labeling and dynamic susceptibility-weighted contrast-enhanced MR imaging.** *Radiology* 2003;228:523–32
13. Kimura H, Takeuchi H, Koshimoto Y, et al. **Perfusion imaging of meningioma by using continuous arterial spin-labeling: comparison with dynamic susceptibility-weighted contrast-enhanced MR images and histopathologic features.** *AJNR Am J Neuroradiol* 2006;27:85–93
14. Kim HS, Kim SY. **A prospective study on the added value of pulsed arterial spin-labeling and apparent diffusion coefficients in the grading of gliomas.** *AJNR Am J Neuroradiol* 2007;28:1693–99
15. Noguchi T, Yoshiura T, Hiwatashi A, et al. **Perfusion imaging of brain tumors using arterial spin-labeling: correlation with histopathologic vascular density.** *AJNR Am J Neuroradiol.* 2008;29:688–93
16. Petersen ET, Lim T, Golay X. **Model-free arterial spin labeling quantification approach for perfusion MRI.** *Magn Reson Med* 2006;55:219–32
17. Petersen ET, Mouridsen K, Golay X, all named co-authors of the QUASAR Test-Retest Study. **The QUASAR reproducibility study. Part II. Results from a multi-center arterial spin labeling test-retest study.** *Neuroimage* 2010;49:104–13
18. Louis DN, Ohgaki H, Wiestler OD, et al. *World Health Organization Classification of Tumours of the Central Nervous System.* Lyon, France: IARC Press; 2007
19. Paulson ES, Schmainda KM. **Comparison of dynamic susceptibility-weighted contrast-enhanced MR methods: recommendations for measuring relative cerebral blood volume in brain tumors.** *Radiology* 2008;249:601–13
20. Wong EC, Buxton RB, Frank LR. **Quantitative imaging of perfusion using a single subtraction (QUIPSS and QUIPSS II).** *Magn Reson Med* 1998;39:702–08
21. Günther M, Bock M, Schad LR. **Arterial spin labeling in combination with a look-locker sampling strategy: inflow turbo-sampling EPI-FAIR (ITS-FAIR).** *Magn Reson Med* 2001;46:974–84
22. Oppo K, Leen E, Angerson WJ, et al. **Doppler perfusion index: an interobserver and intraobserver reproducibility study.** *Radiology* 1998;208:453–57
23. Shrout PE, Fleiss JL. **Intraclass correlations: uses in assessing rater reliability.** *Psychol Bull* 1979;86:420–28
24. Donner A, Zou G. **Testing the equality of dependent intraclass correlation coefficients.** *The Statistician* 2002;51:367–79
25. Fanchin R, Taieb J, Lozano DH, et al. **High reproducibility of serum anti-Mullerian hormone measurements suggests a multi-staged follicular secretion and strengthens its role in the assessment of ovarian follicular status.** *Hum Reprod* 2005;20:923–27
26. Bland JM, Altman DG. **Statistical methods for assessing agreement between two methods of clinical measurement.** *Lancet* 1986;1:307–10
27. Wetzel SG, Cha S, Johnson G, et al. **Relative cerebral blood volume measurements in intracranial mass lesions: interobserver and intraobserver reproducibility study.** *Radiology* 2002;224:797–803
28. Sugahara T, Korogi Y, Kochi M, et al. **Perfusion-sensitive MR imaging of gliomas: comparison between gradient-echo and spin-echo echo-planar imaging techniques.** *AJNR Am J Neuroradiol* 2001;22:1306–15
29. Zaharchuk G. **Theoretical basis of hemodynamic MR imaging techniques to measure cerebral blood volume, cerebral blood flow, and permeability.** *AJNR Am J Neuroradiol* 2007;28:1850–58
30. Thomas DL, Lythgoe MF, Calamante F, et al. **Simultaneous noninvasive measurement of CBF and CBV using double-echo FAIR (DEFAIR).** *Magn Reson Med* 2001;45:853–63
31. Kim T, Kim SG. **Quantification of cerebral arterial blood volume and cerebral blood flow using MRI with modulation of tissue and vessel (MOTIVE) signals.** *Magn Reson Med* 2005;54:333–42
32. Shin JH, Lee HK, Kwun BD, et al. **Using relative cerebral blood flow and volume to evaluate the histopathologic grade of cerebral gliomas: preliminary results.** *AJR Am J Roentgenol* 2002;179:783–89
33. Hakyemez B, Erdogan C, Ercan I, et al. **High-grade and low-grade gliomas: differentiation by using perfusion MR imaging.** *Clin Radiol* 2005;60:493–502
34. Kuo PH, Kanal E, Abu-Alfa AK, et al. **Gadolinium-based MR contrast agents and nephrogenic systemic fibrosis.** *Radiology* 2007;242:647–49